SLAC-PUB-11427
August 2005

Search for Lepton Flavour Violation (LFV) in Three-Body Tau Decays at BaBar

M. Hodgkinson (on behalf of the BaBar collaboration)[a]

[a]High Energy Physics Group, University of Manchester, Oxford Road, Manchester, M13 9PL, United Kingdom

The results of searches for Lepton Flavour Violating (LFV) decays at the BaBar detector located on the PEP-II collider, using data collected at an e^+e^- energy of 10.58 GeV, are presented. Upper limits at 90% Confidence Level (CL) are established in the range 1 - 3 $\times$ 10^{-7} for six $\tau \to lll$ modes using 91.5 fb^{-1} of data and in the range 0.7 - 4.8 $\times$ 10^{-7} for fourteen $\tau \to lhh$ modes using 221.4 fb^{-1} of data. The $\tau \to lhh$ results are preliminary.

1. Introduction

With the known amount of neutrino mixing LFV tau decays are predicted at the 10^{-14} level [1]. Models of physics beyond the Standard Model allow the branching fractions of $\tau \to lll$, where l is an electron or muon, and $\tau \to lhh$, where h is a charged pion or kaon, to be in the range 10^{-20} to 10^{-6} [2]. Therefore LFV decays are sensitive to physics beyond the Standard Model. Prior to the B-Factory era the most stringent limits were established by the CLEO collaboration [3]. They found $\mathcal{B}(\tau^- \to \mu^-\mu^+\mu^-) < 1.9 \times 10^{-6}$ at 90% CL and $\mathcal{B}(\tau^- \to e^+\pi^-\pi^-) < 1.9 \times 10^{-6}$ at 90% CL.

2. The BaBar Detector

The BaBar Detector [4], located at the Stanford Linear Accelerator Center (SLAC), consists of several sub-detectors. A Drift Chamber (DCH) and Silicon Vertex Tracker (SVT) are used in particle identification and track reconstruction. A Caesium Iodide Electromagnetic Calorimeter (EMC) is used to detect energy deposits from neutral and charged particles. The Detector of Imaged Ring Cherenkov Light (DIRC) is used to distinguish charged pions and kaons. The Instrumented Flux Return (IFR) is used in muon and K_L^0 identification.

3. Monte Carlo Samples

The hadronic backgrounds ($b\bar{b}$, $c\bar{c}$ and uds) are generated using the EvtGen [5] Monte Carlo generator. The tau-pair production is simulated by kk2f [6] and the tau decays by TAUOLA [7]. Radiative decays are simulated by the PHOTOS [7] generator. In addition LFV signal samples are generated using a modified version of the TAUOLA package to allow a tau to decay to lll or lhh with a 3-body phase-space distribution. A GEANT4 [8] based simulation is used to include the full detector effects and response.

4. Particle Identification

The efficiencies of particle identification have been measured in data control samples binned in momentum, theta and phi. These can be used to determine the probability of identifying a particle in the LFV signal MC. The efficiency is then calculated as an average over the decay products of the tau.

To identify electrons the track E/P (where E is the energy measured by the EMC and P is the momentum measured in the racking system), the EMC shower shape and the ionisation energy loss (dE/dx) in the DCH are used. The number of IFR hits and the EMC energy deposits are used in muon identification. The $\tau \to lll$ modes

Submitted to Nucl.Phys.Proc.Suppl.

Work supported in part by Department of Energy contract DE-AC02-76SF00515
SLAC, Stanford Univesity, Stanford, CA 94309

have an electron efficiency of 91% with a hadron mis-id rate of 2.2% and a muon efficiency of 63% with a hadron mis-id rate of 4.8%. The $\tau \to lhh$ modes have an electron efficiency of 81% with a hadron mis-id rate of 0.2% and a muon efficiency of 44% with a hadron mis-id rate of 1%. The lhh analysis was performed using improved particle identification algorithms which accounts for some of the difference in efficiencies in between the lll and lhh modes.

Both dE/dx and the Cherenkov angle θ_C are used in kaon and pion identification. The $\tau \to lhh$ modes have a pion efficiency of 92% with a kaon mis-id rate of 12% and a kaon efficiency of 81% with pion mis-id rate of 1.4%.

5. Analysis Technique

The event is first divided into two hemispheres, the signal and tag hemispheres, using the plane normal to the thrust axis (calculated from charged and neutral particles). The tag hemisphere is required to contain one identified track with missing momentum (i.e the track momentum should be less than the τ momentum due to the momentum carried away by the unreconstructed neutrino). The signal hemisphere is required to contain three tracks, with particle identification criteria, invariant mass and energy consitent with each decay mode.. The signal side tracks must be in the combinations lll or lhh. To identify signal candidates two discriminating variables, ΔE and ΔM, are used. ΔM is $M_{Rec} - M_\tau$, where M_{Rec} is the reconstructed invariant mass), and ΔE is $E_{Rec(CM)} - \frac{E_{CM}}{2}$, where $E_{Rec(CM)}$ is the reconstructed total energy of the three tracks. Both of these variables are smeared by detector and radiative effects. A Signal Box (SB) is optimised, to find the best 90% CL upper limit asusming no signal is present, for each decay mode separately. The analysis has been conducted in a blind fashion, without looking in the signal region until after the selection criteria and systematic uncertainties have been finalised. Therefore for the lll modes the upper right corner of the signal region in the ΔM(MeV/c)-ΔE(MeV) is located at (30,50) and the lower left corner at (-70,120) for the $e^-e^+e^-$ and $\mu^-e^+e^-$ modes, (-100,-200) for the $\mu^+e^-e^-$ mode, (-50,-200) for the $e^+\mu^-\mu^-$ mode, (-50,-150) for the $e^-\mu^+\mu^-$ and (-30,-150) for the $\mu^-\mu^+\mu^-$ mode. For the lhh modes the upper right corner is at (50,20) and the lower left corner at (-100,-20) for the μhh modes and (-100,-30) for the ehh modes.

6. Background Suppression

The selection criteria are optimised separetely for each channel. The P_T of all four tracks must have momentum greater than 100 MeV/c and the one-prong momentum must be less than 4.8 GeV/c. These cuts suppress Bhabha and di-muon events. A lepton veto on the one-prong is used in some modes to further suppresses Bhabha and di-muon events. Pairs of tracks consistent with arising from a photon conversion are rejected. For the lhh modes the theta of the missing momentum vector is required to be in the range 14 to 137.5 degrees to suppress QED events and the one prong mass (calculated from the missing momentum and the one-prong track four-momentum) and the must have a mode-dependent lower bound in the range 0.6 - 0.8 GeV to suppress QED events and an upper bound of 1.9 GeV to suppress $q\bar{q}$ and Standard Model tau-pair events. No photons with more than 100 MeV energy are allowed in the event. No lepton on the signal side may be identified as a kaon for all the lll modes and the lhh modes with at least one pion.

7. Background Fits to Data

To estimate the number of background events in the signal box a PDF describing the backgrounds is constructed from the data and MC in the Grand Sideband (GS) region. This region is the ΔE-ΔM plane excluding the SB. A PDF describing the QED backgrounds is constructed from the data because it is not possible to generate Monte Carlo samples of QED backgrounds in sufficient quantities. Further PDFs for the $q\bar{q}$ and the Standard Model tau-pair backgrounds are constructed from the MC. Therefore the PDF

is

$$P_{data} = f_{QED} * P_{QED} + f_{qq} * (1 - f_{QED}) P_{qq} + (1 - f_{QED} - f_{qq} * (1 - f_{QED})) P_{\tau\tau} \quad (1)$$

This PDF is used to calculate the number of background events expected in the signal box

$$N_{BKGR} = N_{GS} * \frac{\int_{SB} P_{data} dM dE}{\int_{GS} P_{data} dM dE} \quad (2)$$

where N_{GS} is the number of events found in the GS. The shape of the PDFs in the *lll* analysis for the $q\bar{q}$ and $\tau^+\tau^-$ are given by the product of $P_M(\Delta_M)$ and $P_E(\Delta_E)$ where $P_M(\Delta_M)$ is the sum of two Gaussians with a common mean and $P_E(\Delta_E)$ is $(1-x)/\sqrt{1+x^2})(1 + ax + bx^2 + cx^3)$. The parameter x is defined to be $(\Delta E - d)/e$. The QED PDF is given by the product of $P_{M'}(\Delta_{M'})$ and $P_{E'}(\Delta_{E'})$, M' and E' being rotated from M and E to better fit the distribution, where $P_{M'}(\Delta_{M'})$ is Crystal Ball [9] function and $P_{E'}(\Delta_{E'})$ is a linear function. In the *lhh* analysis the shape of the PDFs for $q\bar{q}$ are given by the product of $P_{M'}(\Delta_{M'})$ and $P_{E'}(\Delta_{E'})$ where $P_{M'}(\Delta_{M'})$ is a Gaussian and $P_{E'}(\Delta_{E'})$ is the same as the $P_E(\Delta_E)$ component in the *lll*'s $q\bar{q}$ PDF, with the transformation $E \rightarrow E'$ applied. The $\tau^+\tau^-$ backgrounds are parameterised by $P_{M'}(\Delta_{M'})$, which is the product of a Gaussian and a bifurcated Gaussian, and $P_{E'}(\Delta_{E'})$ which has the same form as that used for the *lhh* $q\bar{q}$ background. The coordnates E' and M' in the *lhh* $\tau^+\tau^-$ PDF are rotated without the restriction that the axes should remain orthogonal (which is the case for all the other PDFs with rotated axes in these analyses). The QED backgrounds are negligible in the *lhh* modes and so no PDF for QED backgrounds is included.

8. Results

The published results of the $\tau \rightarrow lll$ [10] analysis are shown in Table 1 and the preliminary results of the $\tau \rightarrow lhh$ [11] analysis are shown in Table 2. Upper Limits, at 90% CL, on the branching fractions are placed at the 10^{-7} level. The ΔE-ΔM plane is shown for all 20 modes, in data and signal MC, in Figures 1 and 2. In the *lll* analysis 3.41 background events were expected and 3 were found. In the *lhh* analysis 11.11 background events were expected and 11 were found.

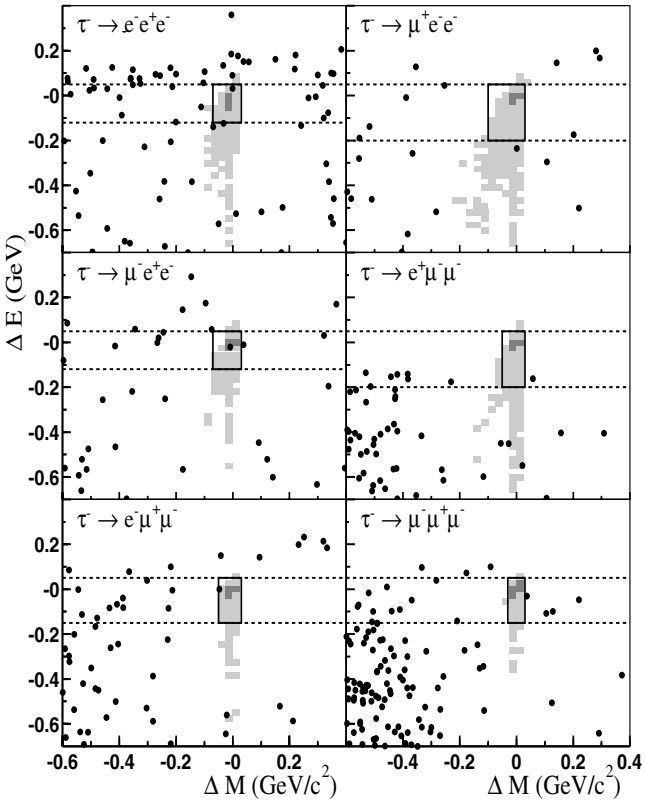

Figure 1. The ΔE-ΔM plane for data (black points) and *lll* signal MC where the dark shading contains 50% of signal events and the light shading 90% of signal events

9. Systematics

The systematic uncertainty on the signal efficiency is dominated by the uncertainty on the PID efficiencies, which comes from the statistical uncertainties in the PID control samples. This uncertainty is mode dependent and ranges from 0.7% to 6.2%. The other two main sources of uncertainty on the signal efficiency are the tracking efficiency, ranging from 2 to 2.5 %, and the sta-

Table 1
Published Results from $\tau \to lll$ (91.5 fb^{-1})

	$\mathcal{B}(e^-e^+e^-)$	$\mathcal{B}(\mu^+e^-e^-)$	$\mathcal{B}(\mu^-e^+e^-)$	$\mathcal{B}(e^+\mu^-\mu^-)$
$\epsilon(\%)$	7.3 ± 0.2	11.6 ± 0.4	7.7 ± 0.3	9.8 ± 0.5
N_{Bgrd}	1.51 ± 0.11	0.37 ± 0.08	0.62 ± 0.10	0.21 ± 0.07
N_{Obs}	1	0	1	0
B_{UL90}	2.0×10^{-7}	1.1×10^{-7}	2.7×10^{-7}	1.3×10^{-7}
	$\mathcal{B}(e^-\mu^+\mu^-)$	$\mathcal{B}(\mu^-\mu^+\mu^-)$		
$\epsilon(\%)$	6.8 ± 0.4	6.7 ± 0.5		
N_{Bgrd}	0.39 ± 0.08	0.31 ± 0.09		
N_{Obs}	1	0		
B_{UL90}	3.3×10^{-7}	1.9×10^{-7}		

Table 2
Preliminary Results from $\tau \to lhh$ (221.5 fb^{-1})

	$\mathcal{B}(e^+K^-K^-)$	$\mathcal{B}(e^+K^-\pi^-)$	$\mathcal{B}(e^+\pi^-\pi^-)$	$\mathcal{B}(\mu^+K^+K^+)$
$\epsilon(\%)$	3.85 ± 0.16	3.19 ± 0.14	3.40 ± 0.15	2.06 ± 0.11
N_{Bgrd}	0.04 ± 0.04	0.16 ± 0.06	0.41 ± 0.10	0.07 ± 0.10
N_{Obs}	0	0	1	1
B_{UL90}	1.5×10^{-7}	1.8×10^{-7}	2.7×10^{-7}	4.8×10^{-7}
	$\mathcal{B}(\mu^+K^-\pi^-)$	$\mathcal{B}(\mu^+\pi^-\pi^-)$	$\mathcal{B}(e^-K^+K^-)$	$\mathcal{B}(e^-K^+\pi^-)$
$\epsilon(\%)$	2.85 ± 0.16	3.30 ± 0.18	3.77 ± 0.16	3.08 ± 0.13
N_{Bgrd}	1.54 ± 0.28	1.46 ± 0.23	0.22 ± 0.06	0.32 ± 0.09
N_{Obs} 1	0	0	0	
B_{UL90}	2.2×10^{-7}	0.7×10^{-7}	1.4×10^{-7}	1.7×10^{-7}
	$\mathcal{B}(e^-\pi^+K^-)$	$\mathcal{B}(e^-\pi^+\pi^-)$	$\mathcal{B}(\mu^-K^+K^-)$	$\mathcal{B}(\mu^-K^+\pi^-)$
$\epsilon(\%)$	3.10 ± 0.13	3.30 ± 0.15	2.16 ± 0.12	2.97 ± 0.16
N_{Bgrd}	0.14 ± 0.06	0.81 ± 0.15	0.24 ± 0.08	1.67 ± 0.32
N_{Obs}	1	0	0	2
B_{UL90}	3.2×10^{-7}	1.2×10^{-7}	2.5×10^{-7}	3.2×10^{-7}
	$\mathcal{B}(\mu^-\pi^+K^-)$	$\mathcal{B}(\mu^-\pi^+\pi^-)$		
$\epsilon(\%)$	2.87 ± 0.16	3.40 ± 0.19		
N_{Bgrd}	1.04 ± 0.20	2.9 ± 0.42		
N_{Obs}	1	3		
B_{UL90}	2.6×10^{-7}	2.9×10^{-7}		

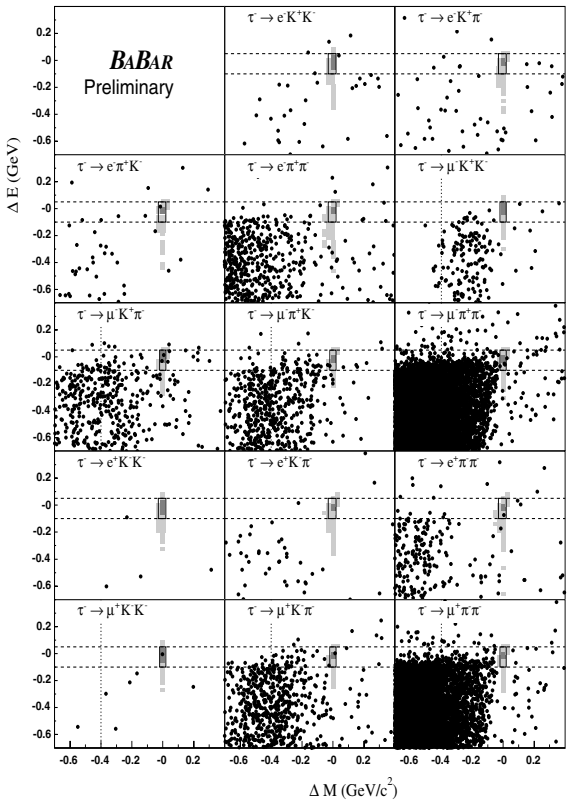

Figure 2. The ΔE-ΔM plane for data (black points) and lhh signal MC where the dark shading contains 50% of signal events and the light shading 90% of signal events

tistical precision of the Monte Carlo sample used which ranges from 1 to 2 %. There is an additional uncertainty because the amounto f background is extracted from the GS in data which is a low statistics sample. This uncertainty varies from 10 % to 25 % depending on the mode under consideration.

10. Conclusions

New limits on the neutrino-less $\tau \to lll$ and $\tau \to lhh$ modes have been presented; all of them having limits at the 10^{-7} level. The limits in the lhh modes are currently the most stringent yet placed, and good agreement is found between the expected number of background events in the SB and the number found. The experimental limits have now breached the upper regions of theoretical predictions. Further measurements at the B-factories with larger data sets can be expected to push the Upper Limits down even further and thus exclude larger regions of parameter space in theoretical models.

REFERENCES

1. X. Pham, Eur. Phys. C 8 (1999) 513.
2. E. Ma, Nucl. Phys. B Proc. Suppl. 123 (2003) 125.
3. D. Bliss et al., Phys. Rev. D 57 (1998) 5903.
4. B. Aubert et al., Nucl.Instrum.Meth A479 (2002) 1, hep-ex/0105044.
5. D. Lange and A. Ryd, CHEP 1998 Proceedings, 1998.
6. S. Jadach, B. Ward and Z. Was, Comp.Phys.Commun 130 (2000) 260.
7. P. Golonka et al., Submitted to Comp.Phys.Commun (2004), hep-ph/0312240.
8. S. Agostinelli et al., Nuc.Meth. and Instr. A506 (2003) 250 .
9. T. Skwarnicki, 1986, DESY-F31-86-02.
10. B. Aubert et al., Phys.Rev.Lett 92 (2004).
11. B. Aubert et al., Tau04 (2004), hep-ex/0409036.